

SPIN STRUCTURE OF THE NUCLEON^a

J.P.NASSALSKI

Sołtan Institute for Nuclear Studies, ul.Hoża 69, 00-861 Warsaw, Poland.

New experimental results on the spin dependent structure functions a_1 and a_2 which are determined from deep-inelastic scattering experiments at CERN, SLAC and DESY are reviewed. The Bjorken sum rule and the singlet axial charge a_0 . Results are discussed in the framework of perturbative QCD. The role of the polarised gluons in the interpretation of the experiments which aim to determine gluon polarisation are shown.

1 Introduction

One of the most exciting problems in high energy physics is to describe the nucleon spin in terms of its partonic constituents: quarks and gluons. The experimental tool which is used is deep-inelastic scattering of leptons on nucleons, from which parton distributions are determined. The theoretical tool is Quantum Chromodynamics (QCD) which describes the dynamics of parton interactions.

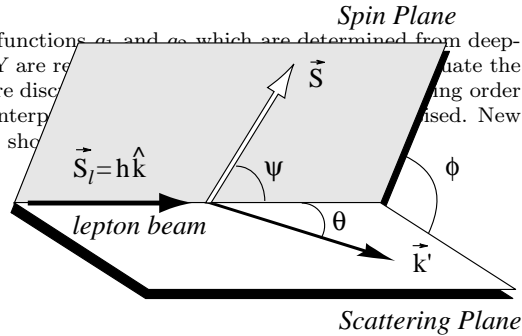
The interest in this subject was initialised by the discovery by the EMC¹ that only a small fraction of the nucleon's spin is carried by quarks. The discovery triggered a large experimental and theoretical activity which is still pursuing.

The main objectives of the present research are focused on the determination and interpretations of the singlet axial charge (a_0) and the Bjorken sum rule (BSR), the former related to the nucleon's spin carried by partons and the latter one regarded as a test of perturbative QCD.

The most recent experimental results are from the SMC at CERN, E142, E143 and E154 at SLAC and HERMES at DESY. There is a large progress on the theoretical side, where next-to-leading order (NLO) perturbative QCD calculations became available. The review of these results and of their interpretations is given below.

2 Determination of g_1 and g_2

The spin-dependent structure functions g_1 and g_2 are determined from deep-inelastic scattering of polarised electrons and muons on polarised proton, deuteron and ^3He targets. The one-photon exchange cross section can be written² in terms of the spin-independent ($\bar{\sigma}$) and the spin-dependent cross-section ($\Delta\sigma$):

Figure 1: Definition of angles ψ and ϕ .

$$\frac{d^3\sigma(\psi)}{dx dQ^2 d\phi} = \frac{d^3\bar{\sigma}}{dx dQ^2 d\phi} + \frac{d^3\Delta\sigma(\psi)}{dx dQ^2 d\phi} \quad (1)$$

where $x = Q^2/(2mv)$ is the Bjorken scaling variable, m is the proton mass, $-Q^2$ and ν are the invariant mass and the energy of the virtual photon in the laboratory system, respectively. The angle ϕ is between the lepton scattering plane and the target spin plane and the angle ψ is between lepton momentum and the target spin as shown in Figure 1.

The two terms can be written as:

$$\begin{aligned} \frac{d^3\bar{\sigma}}{dx dQ^2 d\phi} &= \frac{2\alpha^2}{Q^4} \cdot \\ &\left\{ y^2 \left(1 - \frac{2m_l^2}{Q^2} \right) F_1 + \frac{1}{x} \left(1 - y - \frac{y^2\gamma^2}{4} \right) F_2 \right\} \quad (2) \\ \frac{d^3\Delta\sigma(\psi)}{dx dQ^2 d\phi} &= \frac{4\alpha^2}{Q^4} y \cdot \\ &\left\{ \cos\psi \left[\left(1 - \frac{y}{2} - \frac{y^2\gamma^2}{4} \right) g_1 - \frac{y}{2}\gamma^2 g_2 \right] \right. \\ &\left. - \gamma \sin\psi \sqrt{1 - y - \frac{y^2\gamma^2}{4}} \left(\frac{y}{2}g_1 + g_2 \right) \cos\phi \right\}. \quad (3) \end{aligned}$$

Here F_1 and F_2 are spin-independent structure functions, $y = \nu/E$, where E is incident lepton energy, m_l is the lepton mass and $\gamma^2 = Q^2/\nu^2 = 4x^2m^2/Q^2$ vanishes at large Q^2 . The experiments use longitudinally polarised (polarisation P_b) leptons and measure asymmetries of the cross-sections for opposite orientations of target polarisa-

sations (polarisation P_t):

$$A_{\parallel(\perp)} = \frac{\sigma^{\vec{\leftarrow}(\uparrow)} - \sigma^{\vec{\rightarrow}(\downarrow)}}{\sigma^{\vec{\leftarrow}(\uparrow)} + \sigma^{\vec{\rightarrow}(\downarrow)}} f P_b P_t = \frac{\Delta\sigma_{\parallel(\perp)}}{2 \cdot \bar{\sigma}} f P_b P_t, \quad (4)$$

where \rightarrow (\Rightarrow) denote the beam (target) polarisations and $\bar{\sigma}$ refers to spin-averaged cross-section. The symbols \parallel and \perp indicate longitudinal ($\psi = 0$ or π) and transverse ($\psi = \pi/2$) orientations of the target spin, respectively. In the transverse case the asymmetry is measured between interactions where the scattering plane is at an angle ϕ and $\pi \pm \phi$ (see Fig.1). The dilution factor f accounts for the interactions on the unpolarisable material within the target fiducial volume.

These asymmetries can be written in terms of g_1 and g_2 as

$$\begin{aligned} A_{\parallel} &= \left[\underbrace{\frac{g_1 - \gamma^2 g_2}{F_1}}_{A_1} + \eta\gamma \quad \underbrace{\frac{g_1 + g_2}{F_1}\gamma}_{A_2} \right] D f P_b P_t \\ A_{\perp} &= \left[-\underbrace{\frac{g_1 - \gamma^2 g_2}{F_1}}_{A_1} \xi\gamma + \underbrace{\frac{g_1 + g_2}{F_1}\gamma}_{A_2} \right] d f P_b P_t \end{aligned}$$

where η , ξ , D and d are kinematic factors and A_1 and A_2 are virtual photon asymmetries². Therefore

$$\begin{aligned} g_1 &= (A_1 + \gamma A_2)/(1 + \gamma^2) \\ g_1 + g_2 &= A_2/\gamma \end{aligned} \quad \left. \right\} \cdot F_1$$

where

$$F_1(x, Q^2) = \frac{(1 + \gamma^2) F_2(x, Q^2)}{2x(1 + R(x, Q^2))}.$$

The experiments use the NMC parameterisation³ for F_2 and SLAC parametrisation⁴ for $R = \sigma_L/\sigma_T$, the ratio of photoabsorption cross-sections.

3 Recent experiments.

Recent experiments on polarised deep-inelastic scattering are listed in Table 1. Table 2 indicates distributions which have been determined and also the derived quantities evaluated at fixed values of Q_0^2 ; the first moments $\Gamma_1 = \int_0^1 dx g_1(x, Q_0^2)$, twist-3 matrix elements d_k and the polarised valence ($\Delta u_v, \Delta d_v$) and sea ($\Delta \bar{q}$) quark distributions. The semi-inclusive asymmetries will be discussed in Sec.10.

4 Interpretation of g_1 in the QCD-improved parton model

In the QCD-improved parton model, g_1 is expressed in terms of distribution functions of longitudinal polarisation of partons; quarks (Δq_i) and antiquarks ($\Delta \bar{q}_i$) of flavour i and gluons (Δg). Here $\Delta f \equiv f^+ - f^-$ and $f^{+(-)}$ are distribution functions of partons with spin parallel (antiparallel) to nucleon spin:

$$\begin{aligned} g_1(x, Q^2) = & \frac{1}{2} \sum_{i=1}^{n_f} e_i^2 C_i(x, Q^2) \otimes [\Delta q_i + \Delta \bar{q}_i](x, Q^2) \\ & + C_g(x, Q^2) \otimes \Delta g(x, Q^2), \end{aligned} \quad (5)$$

where n_f is the number of active flavours and $C_{i(g)}$ are quark (gluon) coefficient functions and $C \otimes \Delta f \equiv \int_x^1 \frac{dy}{y} C(\frac{x}{y}, Q^2) \Delta f(y, Q^2)$.

The coefficient functions can be expanded in powers of α_s and at next-to-leading order (NLO) they are:

$$\begin{aligned} C_i(x, Q^2) &= \delta(x-1) + \frac{\alpha_s}{2\pi} C_i^{(1)}(x) + \mathcal{O}(\alpha_s^2) \\ C_g(x, Q^2) &= 0 + \frac{\alpha_s}{2\pi} C_g^{(1)}(x) + \mathcal{O}(\alpha_s^2) \end{aligned} \quad (6)$$

At leading order (LO) we therefore get

$g_1(x) = \frac{1}{2} \sum_i e_i^2 (\Delta q_i(x) + \Delta \bar{q}_i(x))$, which is simply related to $\Delta q = q^+ - q^-$. This can be compared to the spin-averaged structure function $F_1(x) = \frac{1}{2} \sum_i e_i^2 (q_i(x) + \bar{q}_i(x))$ related to the sum $q = q^+ + q^-$.

5 New results on g_1 and g_2

5.1 Results on g_1^p

Figure 2 shows results on $g_1^p(x)$ from the experiment E143⁵ and from an updated (preliminary) analysis of the SMC data⁶. The points are shown at measured $Q^2 > 1 \text{ GeV}^2$. In the overlap region the results agree within the errors. At smaller values of x the SMC points have large errors due to the cut $Q^2 > 1 \text{ GeV}^2$ which eliminates most of the events. Figure 3 shows the corresponding asymmetry $A_1^p = g_1^p/F_1^p$ and also the one (preliminary) obtained with the cut $Q^2 > 0.2 \text{ GeV}^2$; in the latter case the x range is extended down to $x = 0.001$ and the results do not show any large variation with x .

Table 1: Recent experiments on polarised DIS.

Expt.	Beam	(GeV)	Target	P_b	P_t	$f^{(a)}$
SMC <i>in 1996:</i>	μ	190	C_4H_9OH	p	0.8	0.9
		190 ^(b)	C_4D_9OH	d	0.8	0.5
		190	$^{14}NH_3$	p	0.8	0.9
E142	e	19-25	3He	n	0.4	0.3-0.4
E143		10-29	$^{15}NH_3$	p	0.8	0.7
		10-29	$^{15}ND_3$	d	0.8	0.3
E154		49	3He	n	0.8	0.4
E155		49	$^{15}NH_3$	p	0.8	0.7
<i>in 1997:</i>		49	$^{15}ND_3$ (or LiD)	d	0.8	(0.5)
		28	3He	n	0.5	0.5
HERMES <i>in 1996:</i>	e	28	3He	n	0.5	1/3
		28	H_2	p	0.5	0.9
						1

^(a) effective f in the target fiducial volume.

^(b) includes also data at 100 GeV.

Table 2: Distributions determined from polarised DIS.

Distribution	Derrived quantity	Experiment
$g_1^{p(d)}(x, Q^2)$	$\Gamma_1^{p(d)}$	SMC, E143
$g_1^n(x, Q^2)$	Γ_1^n	E142 - being reevaluated E154 (meas. range) HERMES SMC and E143 - from (p, d)
$g_2^{p(d)}(x)$	$d_{k=2,4,6}^{p(d)}$	E143 SMC - $A_{\perp}^{p(d)}$ only
<i>semi-inclusive asymmetries: $(A_{\parallel})^{\pi^+(\pi^-, \pi^+ - \pi^-)}(x)$</i>	$\Delta u_v(x)$ $\Delta d_v(x)$ $\Delta \bar{q}(x)$	SMC

Figure 4 shows the Q^2 -dependence of the asymmetry $A_1^p(x, Q^2)$ from the E143, the SMC and the EMC¹ in bins of x . Within the errors no Q^2 -dependence is seen between the data sets from SLAC and CERN, covering different ranges of Q^2 at fixed x .

5.2 Results on g_1^d

Figure 5 shows results on $g_1^d(x)$ from the experiment E143⁷ and from the SMC (preliminary)⁸. The points are shown at measured $Q^2 > 1 \text{ GeV}^2$. In the overlap region the results agree within the errors.

The Q^2 -dependence of the asymmetry

$A_1^d(x, Q^2)$ obtained from the E143 and the SMC data in the region $Q^2 > 0.2 \text{ GeV}^2$ is shown in Figure 6. Within the errors no variation of the asymmetry A_1^d with Q^2 is observed. Note however, that at the smallest values of x and Q^2 covered by the E143, their analysis⁹ based on all previously published data on $A_1^p(x, Q^2)$ and $A_1^d(x, Q^2)$ indicates a behaviour $A_1^{p(d)}(x, Q^2) \sim (1 + C^{p(d)}(x))/Q^2$.

5.3 Results on g_1^n

The structure function g_1^n is obtained from the measurements of g_1^d and g_1^p (SMC, E143) or from 3He (E142, E154, HERMES). In both cases different corrections are needed, however all data on

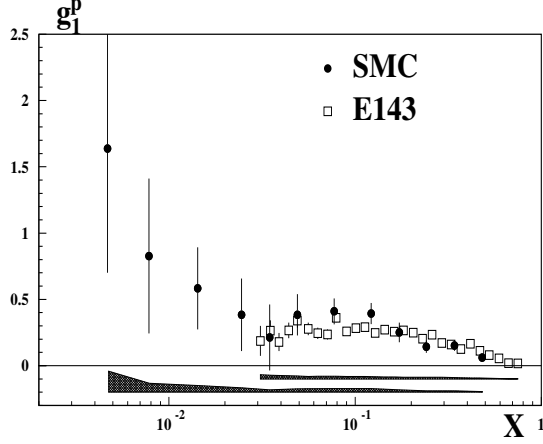


Figure 2: The structure function $g_1^p(x)$ from the SMC (preliminary) and from the E143. Points are shown at measured $Q^2 > 1 \text{ GeV}^2$ with the statistical errors. The sizes of the systematic errors are indicated with the bands.

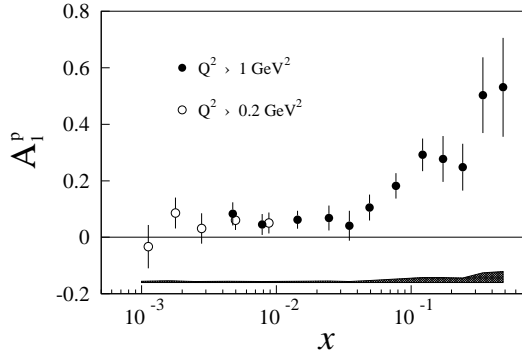


Figure 3: The SMC results on the asymmetry $A_1^p = g_1^p/F_1^p$ for $Q^2 > 1 \text{ GeV}^2$ and $Q^2 > 0.2 \text{ GeV}^2$ (preliminary). The errors are statistical. The size of the systematic errors for the result at $Q^2 > 0.2 \text{ GeV}^2$ is indicated with the band.

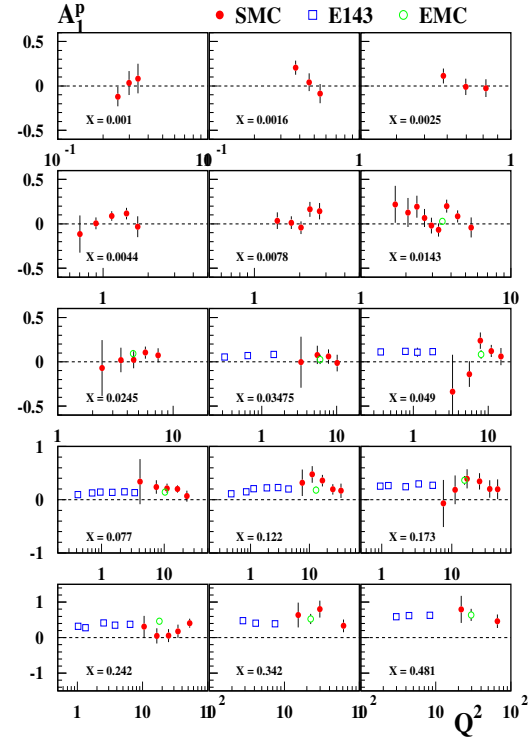


Figure 4: Q^2 dependence of the asymmetry $A_1^p(x, Q^2)$ from the E143, the SMC and the EMC in bins of x . The SMC results are preliminary. Only statistical errors are shown.

g_1^n are consistent, as will be shown below.

Results from deuteron and proton data

In the deuteron, neutron and proton are either in S-state, with both spins in the direction of the deuteron spin, or in D-state where they are opposite to it. The probability of the D-state is $5 \pm 1\%$ ¹⁰ and for the asymmetries the correction is 8%: $A_1^{p+n} = 1.08 A_1^d$. The off-mass shell effects are negligible for $x < 0.7$ ¹¹. Shadowing effects at small x were found to give¹² $A_1^{p+n} = 1.02 A_1^d$ at $x = 0.003$; there are no independent estimates and this correction is not made. Therefore we have $1.08 g_1^d = (g_1^p + g_1^n)/2$.

Figure 7 shows the results for $g_1^n(x)$ from the experiments E143 and SMC (preliminary). In the region of overlap they are consistent, as expected from the agreement on g_1^p and g_1^d . In the region of small x , covered by the SMC data, the spin-dependent structure functions $g_1^n(x)$ and $g_1^p(x)$ have different signs. In the same region the spin-

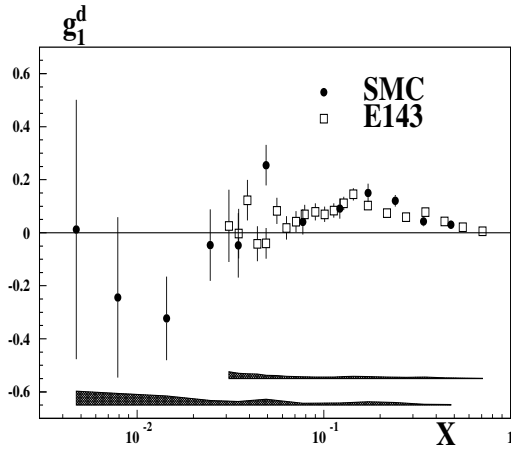


Figure 5: The structure function $g_1^d(x)$ from the SMC at CERN and from the E143 experiment at SLAC. The SMC results are preliminary. Points are shown at measured $Q^2 > 1 \text{ GeV}^2$ with the statistical errors. The sizes of the systematic errors are indicated with the bands.

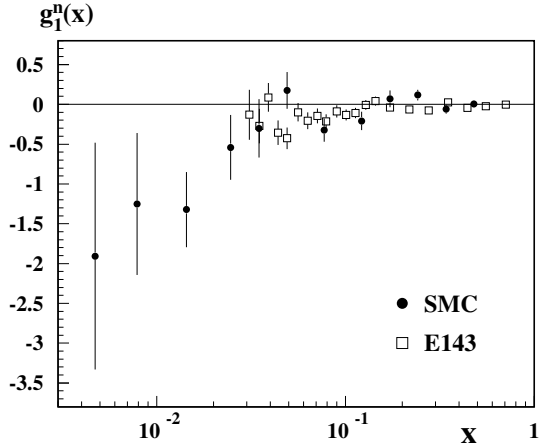


Figure 7: The structure function $g_1^n(x)$ obtained from proton and deuteron data of E143 and SMC (preliminary). The error bars show statistical errors only.

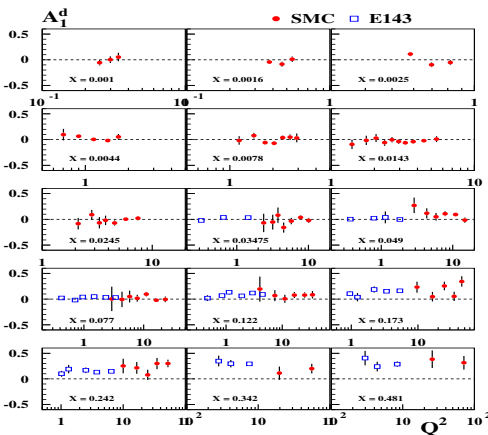


Figure 6: Q^2 dependence of the asymmetry $A_1^d(x, Q^2)$ from the SMC and the E143 in bins of x . SMC Results are preliminary. Only statistical errors are shown.

averaged structure function $F_2^n(x)$ and $F_2^p(x)$ are known¹³ to agree within $\sim 3\%$ which is interpreted as due to predominance of the sea quarks. The difference observed here might indicate a relatively important contribution from polarised valence quarks at small x (see sec.10).

Results from helium data.

In the helium wave function the main configurations are: S-wave with two proton spins in the opposite directions and the neutron spin in the direction of helium spin (87%) and D-wave with neutron spin opposite to it and the two proton spins parallel (3%). No other nuclear corrections are made and $g_1^{^3He} = (0.87g_1^n - 0.03g_1^p)/3$. However, it has been indicated¹⁴ that the effects from an admixture of Δ -isobars and from shadowing might be important both for 3He and for 3H . Nuclear effects in unpolarised 3He will be estimated from measurements of $\sigma^{^3He}/(\sigma^d + \sigma^p)$ by HERMES this year¹⁵.

Figure 8 shows new, preliminary results from the experiment E154 at SLAC¹⁶. In the same figure preliminary results from the reanalysed experiment E142 are also included. There is a good agreement between the two experiments. Results from E154 have very high statistical precision, comparable or better than the systematic one.

New, preliminary results from HERMES experiment¹⁵ are shown in Figure 9.

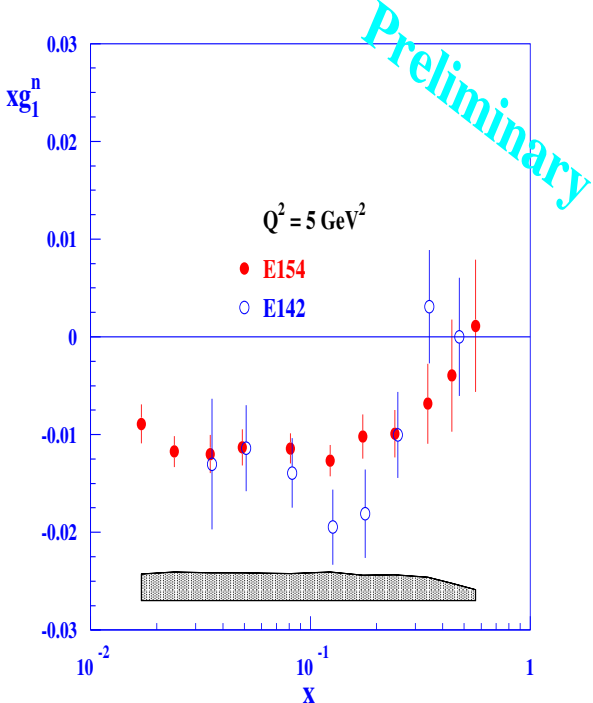


Figure 8: Preliminary results on the structure function $xg_1^n(x)$ from the SLAC experiments E154 and E142 (re-analysed), evaluated at $Q^2 = 10 \text{ GeV}^2$. The error bars show the sizes of statistical errors. The systematic errors of E154 results are shown with the band.

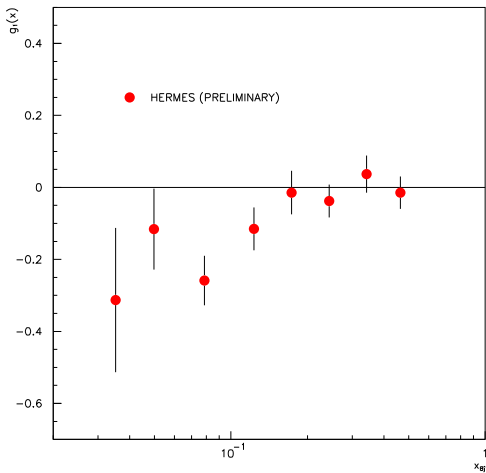


Figure 9: Preliminary results on the structure function $xg_1^n(x)$ from HERMES experiment at DESY. Only systematical errors are shown with the error bars.

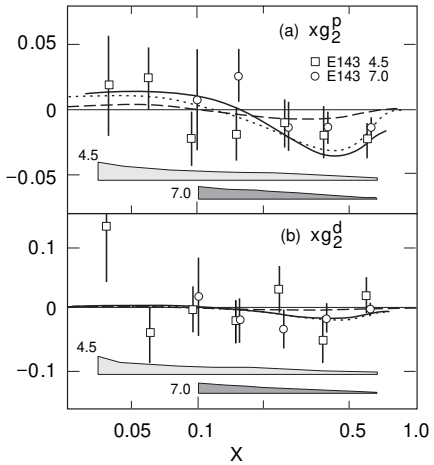


Figure 10: The structure functions $g_2^p(x)$ and $g_2^d(x)$ from the experiment E143. The error bars show the statistical errors. The size of the systematic errors is shown with the band. See text for the explanation of the lines.

6 Results on $g_2^{p(d)}(x)$

Results on $g_2^p(x)$ and $g_2^d(x)$ come from experiment E143¹⁸ and they are shown in Figure 10. The results are given at measured $Q^2 > 1 \text{ GeV}^2$. Assuming the validity of Burkhard-Cottingham sum rule¹⁹, $\int_0^1 g_2(x, Q^2) dx = 0$, g_2 can be written as a sum of the twist-2 term (g_2^{WW}) and a pure twist-3 one (\overline{g}_2): $g_2(x, Q^2) = g_2^{WW}(x, Q^2) + \overline{g}_2(x, Q^2)$. The term g_2^{WW} can be expressed by g_1 (Wandzura and Wilczek²⁰):

$$g_2^{WW}(x, Q^2) = -g_1(x, Q^2) + \int_x^1 \frac{g_1(y, Q^2)}{y} dy. \quad (7)$$

The solid line in the figure represents g_2^{WW} . It is consistent with the data indicating that twist-3 term is small.

At smaller values of x there are measurements of $A_2^{p(d)}(x)$ from the SMC²¹. Results on $A_2^p(x)$ are shown in Figure 11 together with the results from the E143 experiment. Also shown are the SMC results obtained with the cut $Q^2 > 0.5 \text{ GeV}^2$. The solid line in the figure represents an upper limit of $A_2(x)$ given by \sqrt{R} . The present measurements fall substantially below this limit.

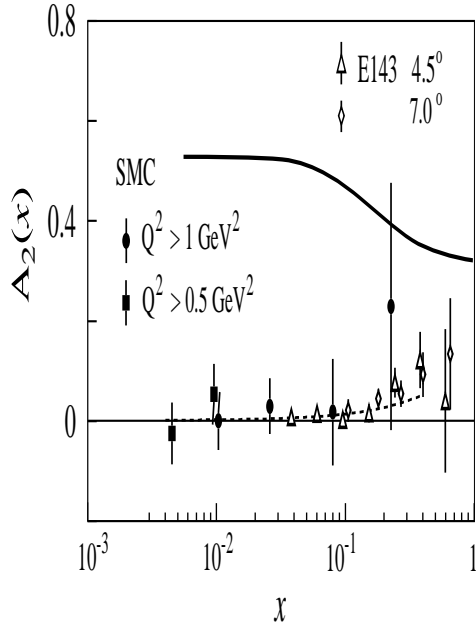


Figure 11: The asymmetry $A_2^p(x)$ from the SMC and from the E143. Only statistical errors are shown. See text for the explanation of the line.

7 The first moment $\Gamma_1(Q_0^2)$

The main physics interest is in the first moments of the the spin-dependent structure functions g_1 :

$$\Gamma_1(Q_0^2) = \int_0^1 g_1(x, Q_0^2) dx \quad (8)$$

where Γ_1 is the leading-twist (LT) term in the operator product expansion.

In the experiments g_1 is determined in a finite range of x , where x and $\langle Q^2(x) \rangle$ are correlated. Therefore calculation of Γ_1 involves extrapolation of measured $g_1(x, Q^2)$ to a common Q_0^2 and also extrapolation to $x = 0$ and $x = 1$. Finally, in order to evaluate the LT contribution to Γ_1 , corrections due to higher-twist terms are required.

7.1 Theoretical interpretation

The first moment of $g_1(x, Q^2)$ can be written as

$$\begin{aligned} \Gamma_1(Q^2) &= \frac{1}{2} [C_{NS}(Q^2)a_{NS} + \\ &\quad \langle e^2 \rangle C_S(Q^2)a_0(Q^2)] \end{aligned} \quad (9)$$

in terms of the singlet (S) and non-singlet (NS) axial charges a_i ,

$$ms^\mu a_i = \langle \text{target}, p, \text{spin} | J_{5i}^\mu | \text{target}, p, \text{spin} \rangle,$$

of quark axial-vector current, $J_{5i}^\mu = \bar{\psi}_i \gamma^\mu \gamma_5 \psi_i$, and Wilson coefficient functions $C_{S(NS)}$ where p is the target momentum. In the Quark-Parton Model (QPM) the axial charge of a quark of flavour f is expressed in terms of the integral of the corresponding distribution functions of quark polarisations: $\Delta q_f(Q^2) \equiv \int \Delta q_f(x, Q^2) dx \equiv a_f$. The non-singlet axial charge,

$$a_{NS} = \sum_{i=1}^{n_f} (e_i^2 - \langle e^2 \rangle a_i),$$

is conserved and, assuming $SU(3)_f$ symmetry, it can be written in terms of F and D constants in hyperon β -decays:

$$\begin{aligned} a_{NS} &= \frac{1}{6} \underbrace{(a_u - a_d)}_{a_3 = |g_A| = F + D} + \frac{1}{18} \underbrace{(a_u + a_d - 2a_s)}_{a_8 = 3F - D} + \\ &\quad \underbrace{(a_u + a_d + a_s - 3a_c)}_{\text{if } Q^2 > m_c^2}. \end{aligned} \quad (10)$$

The singlet axial charge $a_0(Q^2)$ is not conserved because at two loops the gluon operator mixes with divergence of the singlet axial-vector current (this is called "axial anomaly"). As a result, the decomposition of a_0 depends on the renormalisation scheme:

$$a_0(Q^2) = \begin{cases} \text{in } \overline{\text{MS}} \text{ scheme :} \\ \sum_i (\Delta q_i + \Delta \bar{q}_i)(Q^2) = \\ \Delta u_v + \Delta d_v + 2 \sum_i \Delta \bar{q}_i(Q^2) \\ \text{in Adler - Bardeen (AB) scheme :} \\ \sum_i (\Delta q_i + \Delta \bar{q}_i) - n_f \frac{\alpha_s(Q^2)}{2\pi} \Delta G(Q^2), \end{cases} \quad (11)$$

where $\Delta G(Q^2) = \int \Delta g(x, Q^2) dx$ is the integrated gluon polarisation. The gluon polarisation enters explicitly in AB scheme³⁵ while in $\overline{\text{MS}}$ scheme it contributes via polarised sea $\Delta \bar{q}_i(Q^2)$.

7.2 Evolution of g_1 with Q^2

The structure function g_1 (Eq.5) can be expressed in terms of the singlet and non-singlet polarised parton distribution functions:

$$\begin{aligned} g_1(x, Q^2) &= \frac{\langle e^2 \rangle}{2} [C_{NS} \otimes \Delta q_{NS} + \\ &\quad C_S \otimes \Delta q_S + 2n_f C_g \otimes \Delta g] \end{aligned} \quad (12)$$

where

$$\Delta q_{NS} = \sum_{i=1}^{n_f} \left(\frac{e_i^2}{\langle e^2 \rangle} - 1 \right) (\Delta q_i + \Delta \bar{q}_i) \text{ and}$$

$$\Delta q_S = \sum_{i=1}^{n_f} (\Delta q_i + \Delta \bar{q}_i).$$

and they evolve according to the Altarelli-Parisi equations:

$$\frac{d}{d \ln t} \Delta q_{NS} = \frac{\alpha_s(t)}{2\pi} \Delta P_{NS}^{qq} \otimes \Delta q_{NS} \quad (13)$$

$$\frac{d}{d \ln t} \begin{pmatrix} \Delta q_S \\ \Delta g \end{pmatrix} = \frac{\alpha_s(t)}{2\pi} \begin{pmatrix} \Delta P_S^{qq} & 2n_f \Delta P_S^{gg} \\ \Delta P_S^{gq} & \Delta P_S^{gg} \end{pmatrix} \otimes \begin{pmatrix} \Delta q_S \\ \Delta g \end{pmatrix}, \quad (14)$$

where $t = \ln(Q^2/\Lambda^2)$. The splitting functions $\Delta P^{ij} \equiv P^{i^+ j^+} - P^{i^+ j^-}$ at next-to-leading order,

$$P(x, Q^2) = P^{(0)}(x) + \frac{\alpha_s(Q^2)}{2\pi} P^{(1)}(x),$$

have recently been calculated²². Differences between spin-dependent and spin-averaged splitting functions give rise to different Q^2 -evolutions of g_1 and F_1 . Therefore the assumption made in most of the analyses up to now that $A_1 = g_1/F_1$ is independent of Q^2 , is strictly not valid.

7.3 Extrapolation of g_1 in x

Extrapolations of $g_1(x, Q_0^2)$ at large x , from $x_{max} \sim 0.7$ to $x = 1$, were made assuming $g_1(x) \sim F_1(x)$ or $\sim (1-x)^3$ or assuming $A_1(x \rightarrow 1) \rightarrow 1$. The resulting contributions to Γ_1 are very small and therefore this subject is not controversial.

However, extrapolation at small x , from $x_{min} = 0.003$ for the SMC data and ~ 0.03 for experiments at SLAC and DESY to $x = 0$ requires phenomenological input for the behaviour of the dominant singlet contribution. This behaviour depends on the interplay between expectations from

- Regge trajectories (a_1 and f_1), $g_1(x) \sim x^\alpha$, $0 \leq \alpha \leq 0.5$, used by the SMC, E142, E143 and HERMES,
- non-perturbative Pomeron²³, $g_1(x) \sim \log(1/x)$, alternatively used by the E143,

and the expectations from perturbative QCD which were not used in the experimental analyses:

- $|g_1(x)|$ rises faster than $\sim \log(1/x)^\nu$ for any ν and slower than $\sim 1/x^\lambda$ for any $\lambda > 0$ ³⁵
- $g_1(x) \sim 1/x^\omega$ with $\omega > 1$ for $\alpha_s > 0.12$, where a strong rise of $g_1(x)$ at small x is possible²⁴.

Experiments assign a 100% error to their extrapolations at small x but the question of underlying assumptions is not settled; measurements of g_1 at smaller x are needed. The need to have small extrapolation error is clearly visible in very high statistics E154 data on g_1^n .

7.4 Higher-twist terms

In the operator product expansion Γ_1 is given by

$$\begin{aligned} \Gamma_1(Q^2) = & \Gamma_1^{LT}(Q^2) + \\ & \underbrace{\frac{m^2}{9Q^2} \left[a^{(2)} + 4d^{(2)} + 4f^{(2)} \right]}_{C_{HT}/Q^2} + \\ & \mathcal{O}\left(\frac{m^4}{Q^4}\right) \end{aligned} \quad (15)$$

where $a^{(2)}$, $d^{(2)}$ and $f^{(2)}$ are the matrix elements of twist-2, twist-3 and twist-4 operators, respectively.

There are first experimental results¹⁸ from E143 on $a_{p(d)}^{(2)}$ and $d_{p(d)}^{(2)}$. They require $g_2(x)$ as input and have large statistical errors.

Phenomenological estimates of their magnitude come from QCD sum rules, renormalon methods, lattice QCD and from MIT bag model (see Ref. ²⁵ for a review and also Ref. ²⁶). Their values differ, even in sign. However, the implied corrections to Γ_1 are in general smaller than the experimental errors. They are also less important at higher Q^2 .

7.5 Results for Γ_1

Recent experimental results for Γ_1 are shown in Table 3. They were obtained under the assumption that A_1 is independent of Q^2 and using Regge-type extrapolations of g_1 to $x = 0$.

Table 3: Experimental results for the first moments of the spin-dependent structure functions. The values in parentheses give the statistical and the systematic error, respectively. Except for the E143, all results are preliminary. E142 results are from Ref.¹⁷.

Experiment	Q^2 (GeV 2)	Γ_1^p	Γ_1^d	Γ_1^n
SMC	10	0.136(14)(9)	0.038(7)(5)	-0.055 (24) ^{a)}
E143	3	0.127(4)(10)	0.042(3)(4)	-0.037(8)(11) ^{a)}
E142	2	—	—	-0.031(6)(9)
HERMES	3	—	—	-0.032(13)(17)
E154	5	—	—	-0.037(4)(10) ^{b)}

^(a) from deuteron and proton data.

^(b) in the measured range only ($0.014 < x < 0.7$).

8 Physics interest in Γ_1

The first moments of the spin-dependent structure functions g_1^p and g_1^n are used to test the fundamental Bjorken sum rule²⁷. Furthermore, Γ_1 is used to evaluate the singlet element of the axial-vector current, a_0 . In the leading-order it is equal to the total spin carried by quarks, $a_0 = \Delta\Sigma$, and its value was predicted using the Ellis-Jaffe sum rule²⁸. The value found by the EMC¹ was much smaller than the prediction. This discovery has led to the "spin crisis" and triggered large experimental and theoretical activity.

8.1 Bjorken sum rule

Under the assumption of the isospin symmetry between neutron and proton we can write for the axial charges:

$$a_u^n = a_d^p, \quad a_d^n = a_u^p, \quad \text{and} \quad a_q^n = a_q^p; \quad q = s, c, b, t.$$

The singlet term cancels in the difference $\Gamma_1^p - \Gamma_1^n$ (see Eq.9) and we obtain the Bjorken sum rule (BSR) prediction:

$$(\Gamma_1^p - \Gamma_1^n)(Q^2) = \frac{1}{6} C_{NS}(\alpha_s(Q^2)) \cdot |g_A|. \quad (16)$$

This is a very accurate prediction: the value of $|g_A|$, the coupling constant in neutron beta-decay, is known to within 2 permille³¹ and the perturbative expansion of C_{NS} is known to $\mathcal{O}(\alpha_s^3)$ ²⁹ and there is also an estimate of $\mathcal{O}(\alpha_s^4)$ term³⁰. Therefore it is regarded as a test of perturbative QCD. Conversely, since the perturbative expansion is sensitive to the value of α_s , the BSR can be used to determine $\alpha_s(M_Z^2)$.

Table 4: Experimental results for the Bjorken sum. Except for the E143, all results are preliminary. The value in parentheses gives the total error. For Γ_1^n from E142 we use result from Ref.¹⁷

Experiment	Q^2 (GeV 2)	$\Gamma_1^p - \Gamma_1^n$
SMC	10	0.191(36)
E143	3	0.163(19)
E143/E142	3	0.159(14)

Theoretical uncertainties were discussed above; they are due to the assumptions used to obtain $\Gamma_1^{p(n)}$ and to the contributions from higher-twists, C_{HT}^{p-n}/Q^2 .

8.2 Experimental results for the Bjorken sum

The experimental results for the Bjorken sum are given in Table 4. They are compared to the predictions in Figure 12 where we used $n_f = 3$ and $\alpha(M_Z^2) = 0.117 \pm 0.005$. Good agreement with the prediction is observed.

8.3 Determination of α_s

Figure 12 shows also the sensitivity of the predictions to the value of α_s ; the spread in the predictions is mainly due to its error. It is therefore tempting to derive the value of $\alpha_s(M_Z^2)$ from the experimental results on the Bjorken sum, assuming that the prediction given by Eq.16 holds precisely. Since all known terms of the perturbative expansion are negative such procedure re-

Table 5: Results for $(\Delta\Sigma)_{inv.}$ and for Δs .

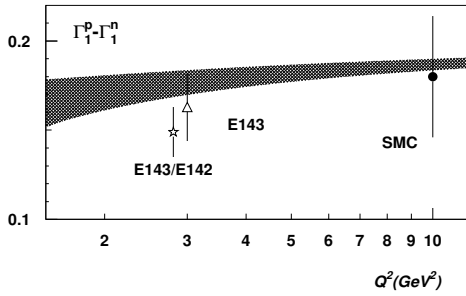


Figure 12: Results for Bjorken sum from recent experiments. The shaded area indicates the predictions.

quires an estimate of the contribution from all higher order terms. The most recent determination³³ of α_s from BSR relies on Padé summation: using an estimate of the average experimental value $(\Gamma_1^p - \Gamma_1^n)(3 \text{ GeV}^2) = 0.160 \pm 0.014$ and $C_{HT}^{p-n} = -0.02 \pm 0.01$, the authors obtain

$$\alpha_s(M_Z^2) = 0.117^{+0.004}_{-0.007} \text{ (exp.)} \pm 0.002 \text{ (th.)}.$$

The theoretical error is mainly due to a renormalisation scale dependence and it is very small.

8.4 Results for a_0 and for the Ellis-Jaffe sum rule

The value of the singlet axial charge (a_0) is obtained from Eq.(9) using experimental values for Γ_1 ; a_{NS} is calculated from g_A and from F and D values³² using Eq.(10) and C_S has been evaluated³⁴ up to $\mathcal{O}(\alpha_s^2)$. It can be written as³⁴:

$$a_0(Q^2) = [1 + c_1 \alpha_s(Q^2) + c_2 \alpha_s^2(Q^2)] \cdot (a_0)_{inv.}$$

where c_i are numerical constants and $(a_0)_{inv.} \equiv a_0(Q^2 \rightarrow \infty)$. Using a_0 interpretation from the \overline{MS} -scheme (Eq.(11)), $a_0(Q^2) \equiv \Delta\Sigma(Q^2)$ is the total spin carried by all quarks. With this interpretation and under the assumption of the flavour symmetry in the polarised sea, the value of $a_s \equiv \Delta s$ can be calculated.

In the leading-order $\Delta\Sigma$ is invariant. Its value can be predicted assuming Ellis-Jaffe assumption

Experiment	$(\Delta\Sigma)_{inv.}$	Δs
SMC	p	0.21 (16)
	d	0.24 (8)
E143	p	0.24 (10)
	d	0.30 (5)

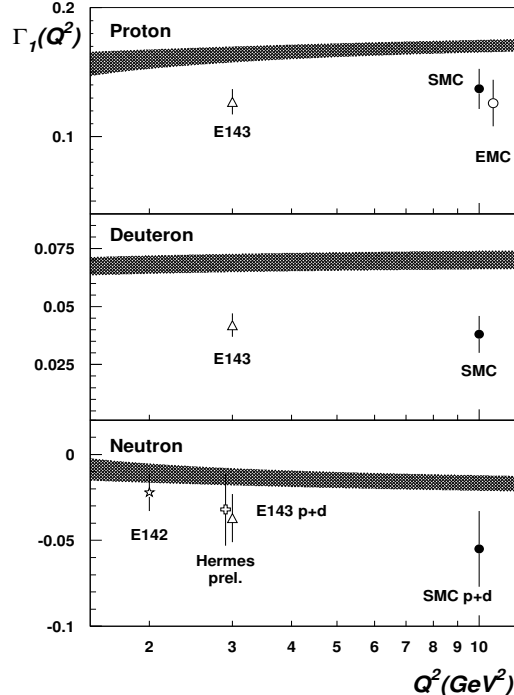


Figure 13: Comparison of the first moments Γ_1 to the Ellis-Jaffe sum rule prediction. Also plotted is the first result from the EMC which gave rise to "the spin crisis".

that OZI rule is valid ($\Delta s = 0$): $\Delta\Sigma = \Delta u + \Delta d = a_8 = 3F - D \simeq 0.6$.

The values of $(\Delta\Sigma)_{inv.}$ and Δs are given in Table 5. Clearly, $\Delta\Sigma$ is below expectation and the OZI rule is violated. An alternative way to demonstrate this discrepancy is to compare Γ_1 to the value predicted under the assumption of $\Delta s = 0$ (Ellis-Jaffe sum rule). With this assumption we have $a_0 = a_8$ and

$$\begin{aligned} (\Gamma_1^{p(n)})_{EJ}(Q^2) &= C_{NS}(Q^2) \left(\pm \frac{1}{12} a_3 + \frac{1}{36} a_8 \right) + \\ &\quad \frac{1}{9} C_S(Q^2) a_8. \end{aligned} \quad (17)$$

Figure 13 clearly shows that a_0 should be bigger than a_8 which requires $a_s < 0$.

8.5 Present understanding of a_0

We can rewrite Eq.(11) in the form:

$$a_0(Q^2) = \begin{cases} \overline{\text{MS}}; \Delta G \text{ enters via polarised sea :} \\ \frac{\Delta \Sigma(Q^2)}{\Delta \Sigma(Q^2)} \\ \overline{\text{AB}}; \Delta G \text{ enters explicitly :} \\ \frac{\Delta \Sigma - n_f \frac{\alpha_s(Q^2)}{2\pi} \Delta G(Q^2)}{\sim Q^2 - \text{independent}} \end{cases} \quad (18)$$

In the AB-scheme, where gluon polarisation enters explicitly, one can estimate ΔG required in order to obtain $\Delta \Sigma = 0.6$; from Eq.18 we obtain $\Delta G(10 \text{ GeV}^2) \sim 2$.

To summarise: the physics interpretation of a_0 in the NLO is scheme-dependent. Its value is below the expectation from the LO due to gluon polarisation.

9 Determinations of ΔG

Indirect determinations of ΔG come from fits of parametrised polarised parton distributions to all $g_1^{p(d,n)}$ data, using the Altarelli-Parisi evolution equations (Eqs.13 and 14) in the NLO. There are three independent analyses^{35 36 37} and in the range $1 < Q^2 < 10 \text{ GeV}^2$ they all require $\Delta G \sim 1 \div 2$.

Sizeable gluon polarisation clearly affects the Q^2 -dependence of g_1 . Since the calculation of $\Gamma_1(Q_0^2)$ requires the extrapolations of $g_1(x, Q_{\text{meas.}}^2) \rightarrow g_1(x, Q_0^2)$, it might lead to different value of Γ_1 . Figures 14 and 15 show the preliminary results from the NLO QCD fits made by the SMC to the recent E143 and SMC data on g_1^p and g_1^d using the procedure of Ref. ³⁵. Lines show the pattern of the Q^2 -dependence ; the solid line shows fitted g_1 at Q^2 measured by the SMC, dashed and dotted lines are the values at Q^2 of 1 GeV^2 and 10 GeV^2 , respectively. Using the extrapolation

$$g_1(x, Q_0^2) = g_1(x, Q_{\text{meas.}}^2) + [g_1(x, Q_0^2) - g_1(x, Q_{\text{meas.}}^2)]_{\text{from fit}} \quad (19)$$

the SMC obtains (preliminary) at $Q_0^2 = 10 \text{ GeV}^2$:

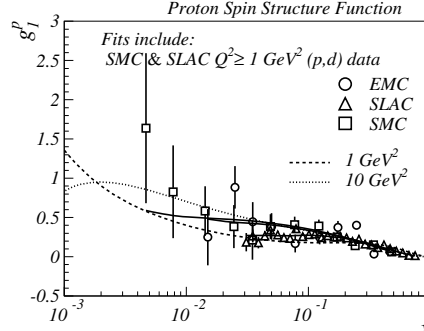


Figure 14: g_1^p from the NLO QCD fits to $g_1^p(x, Q^2)$ and $g_1^d(x, Q^2)$ from the E143 and the SMC. Points show $g_1^p(x)$ at measured Q^2 . See text for explanations.

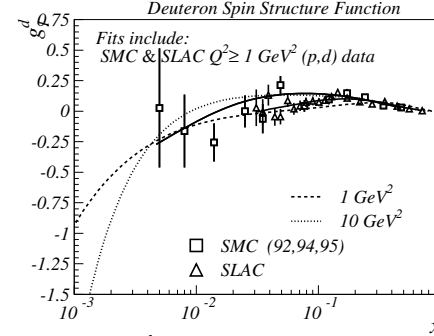


Figure 15: g_1^d from the NLO QCD fits to $g_1^p(x, Q^2)$ and $g_1^d(x, Q^2)$ from the E143 and the SMC. Points show $g_1^d(x)$ at measured Q^2 . See text for explanations.

- $\Gamma_1^p = 0.130 \quad (0.136 \pm 0.017)$
- $\Gamma_1^d = 0.037 \quad (0.038 \pm 0.009)$

where the values given in parentheses are from Table 3 and they were evaluated assuming that g_1/F_1 does not depend on Q^2 .

The theoretical error of Γ_1 due to uncertainty in $\Delta g(x, Q_0^2)$ and to unknown higher-order corrections was estimated³⁵ to be $^{+0.009}_{-0.005}$.

10 Results on the polarised quark distributions

First results on the polarised quark distributions were obtained by the SMC³⁸ from the analysis of asymmetries of semi-inclusive and inclusive cross sections. There are new (preliminary) results from the SMC which include new deuteron data.

The results are obtained assuming QPM. The asymmetry of inclusive virtual photon absorption cross sections is written in terms of the distribution functions of quarks ($q(x, Q^2)$) and of their spin ($\Delta q(x, Q^2)$):

$$A_1(x, Q^2) = \frac{\sum_q e_q^2 \Delta q(x, Q^2)}{\sum_q e_q^2 q(x, Q^2)}. \quad (20)$$

The asymmetry of semi-inclusive cross sections depends also on the fragmentation functions of quarks q into a final state hadron h , $D_q^h(z, Q^2)$, where z is the fraction of quark's energy taken by a hadron. The SMC has determined semi-inclusive asymmetries for the positive and negative hadron yields integrated over $0.2 < z < 1$, $D_q^h(Q^2) = \int_{0.2}^1 D_q^h(z, Q^2) dz$:

$$A_1^{+(-)}(x, Q^2) = \frac{\sum_{q,h} e_q^2 \Delta q(x, Q^2) D_q^h(Q^2)}{\sum_{q,h} e_q^2 q(x, Q^2) D_q^h(Q^2)}. \quad (21)$$

In Eqs. 20 and 21 quark distributions were taken from the MRS parametrisation³⁹ and the fragmentation functions of non-strange quarks into pions were obtained from the EMC measurements⁴⁰ by using charge conjugation and isospin symmetry. In each bin of x these equations for proton and deuteron targets constitute a system of $2 + 4$ linear equations written in terms of three unknown spin distribution: of valence quarks, $\Delta u_v(x)$ and $\Delta d_v(x)$, and of the sea antiquarks, $\Delta \bar{q}(x)$. They were evaluated by the least-square method and the results are shown in Fig. 16. We observe that $\Delta u_v(x)$ is positive while $\Delta d_v(x)$ is negative. The spin distribution of the non-strange sea $\Delta \bar{q}(x)$ is compatible with zero even at small x where the unpolarised sea is large. There is an indication of a non-vanishing valence quark polarisation $\Delta q_v/q_v$ at small x which is consistent with the observation of $g_1^n \neq g_1^p$ at the smallest x in the SMC data.

11 How the proton spins?

In terms of the nucleon constituents we expect:

$$\frac{1}{2} = \frac{1}{2} \Delta \Sigma + \Delta G(Q^2) + L_z(Q^2), \quad (22)$$

where the Q^2 -evolution of $\Delta G(Q^2)$ and $L_z(Q^2)$, the orbital angular momentum of quarks and gluons, must be coupled. This issue raises theoretical activity⁴¹ but it is still under discussion. As discussed in previous sections, the OZI rule gives $\Delta \Sigma \sim 0.6$, which requires $\Delta G(Q^2 = 10 \text{ GeV}^2) \sim 2$ and the equation above leads to $L_z \sim -1.8$.

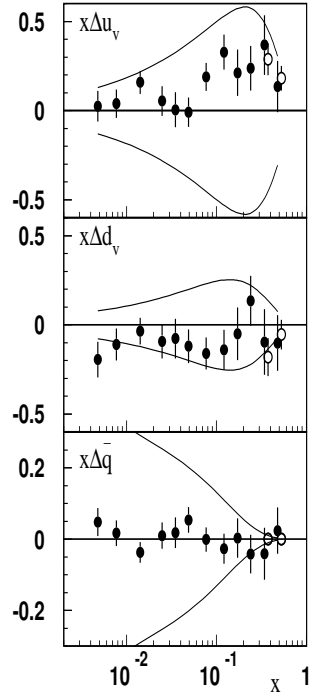


Figure 16: Quark spin distribution functions (a) $x\Delta u_v(x)$, (b) $x\Delta d_v(x)$, (c) $x\Delta \bar{q}(x)$. The open circles are obtained when the sea polarisation is set to zero while the closed circles are obtained without this assumption. The error bars are statistical. The curves correspond to the upper and the lower limits $\pm q(x)$ from the unpolarised quark distributions evaluated at $Q^2 = 10 \text{ GeV}^2$.

12 Prospects for polarised deep-inelastic scattering

12.1 New results from the approved experiments

In the near future we can expect new results from the following experiments:

- SMC will have more data on g_1^p and Δq . There might be new results for $Q^2 < 1 \text{ GeV}^2$ and $x < 0.003$,
- E155 will have new high precision data on $g_1^{p(d)}$ for $Q^2 > 1 \text{ GeV}^2$ and $x > 0.014$,
- HERMES will have new data on Δq (with identified hadrons) and also on $g_1^{p(n,d)}$.

These data will certainly increase the precision of the present results and might produce new, interesting observations. However they will not solve two outstanding problems which came up recently,

1. to determine the shape of $g_1(x)$ at smaller x and $Q^2 > 1 \text{ GeV}^2$,
2. to determine directly gluon polarisation $\Delta g(x)$,

which can be solved only by new experiments.

12.2 Proposed experiments

COMPASS at CERN

Experiment has been proposed on the muon beam line at CERN and recently recommended by the SPSL Committee. The main subject of the deep-inelastic scattering part of the program is to determine $\Delta g/g$ from asymmetries of cross sections for open charm production, $D^0(\bar{D}^0)$:

$$A_{\gamma N}^{c\bar{c}}(\nu) = \frac{\int_{4m_c^2}^{2M\nu} d\hat{s} \Delta\sigma(\hat{s}) \Delta g(x_g, \hat{s})}{\int_{4m_c^2}^{2M\nu} d\hat{s} \sigma(\hat{s}) g(x_g, \hat{s})}. \quad (23)$$

where $\hat{s} = (q+k)^2$, $x_g = \hat{s}/2M\nu$ denotes the nucleon momentum fraction carried by the gluon and $\Delta\sigma$ is the spin-dependent part of the charm production cross section in the photon-gluon process, shown in Figure 17. Using 100 GeV μ -beam the experiment will cover $x_g > 0.07$ where the accuracy $\delta A^{c\bar{c}} \sim 0.05$ is expected. The corresponding accuracy in gluon polarisation is $\delta(\Delta G/G) \sim 0.14$.

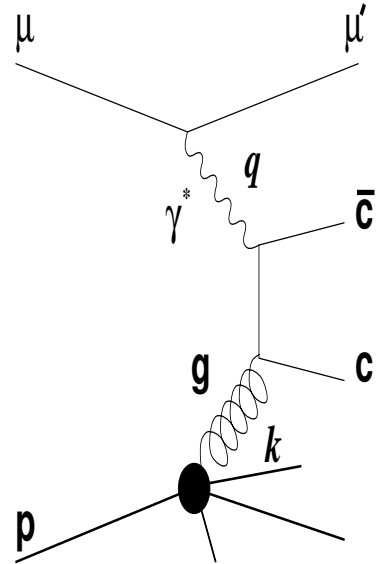


Figure 17: The photon-gluon fusion diagram.

The experiment is expected to start data taking around the year 2000.

Similar experiment on the electron beam at SLAC is being discussed.

At polarised HERA

At HERA the polarised deep-inelastic physics is feasible⁴² with the present H1 and ZEUS detectors if the integrated luminosity $\int \mathcal{L} dt \sim 200 pb^{-1}$ is reached for electron and proton polarisations ~ 0.7 . Three physics items are considered.

1. Δg from di-jet (2+1) events:

These events are produced via photon-gluon fusion process shown in Figure 17, where two jets arise from quark pairs. The momentum fraction carried by the gluon can be determined from \hat{s} , $x_g = x(1 + \hat{s}/Q^2)$, where x is the Bjorken's variable. The expected asymmetries of cross sections are ~ 0.03 and they can be measured to a high accuracy⁴³.

2. Δg from Q^2 -evolution of $g_1(x, Q^2)$:

The measurements cover $x \geq 10^{-4}$ with Q^2 bigger by a factor of 100 compared to fixed-target experiments. However the expected asymmetries are small ($\sim 5 \cdot 10^{-4}$) and the kinematic depolarisation factor is unfavourable.

3. Polarisation of quarks from $g_5^{W^-(W^+)}$:

It has been proposed⁴⁴ to study polarised charge-current processes using both e^-p and e^+p interactions in order to determine new polarised structure functions $g_5^{W^-(W^+)}$. They are expressed by different flavour combinations compared to g_1 , e.g. $g_5^{W^-} + g_5^{W^+} = \Delta u_v + \Delta d_v$. For $x > 0.1$ very large asymmetries (bigger than 0.1) are expected.

The feasibility to have polarised protons at HERA is under study. The possible time scale is most likely to be beyond year 2004.

13 Conclusions

There is a good agreement between experiments at SLAC, CERN and DESY on the results on $g_1^{p(d,n)}$. The Bjorken sum holds well and is being used to determine α_s which might have small theoretical error.

New results are consistent with the singlet axial charge $a_0 \simeq 0.25$ which is below the expectation from the OZI rule and corresponds to $a_s \simeq -0.1$.

On the theoretical side, there is a large progress in understanding this effect in terms of the polarisation of gluons, $\Delta G \sim 1 \div 2$ at $Q^2 \sim 10 \text{ GeV}^2$. However with the present data is not sufficient to determine it more precisely from the scaling violations alone. It might be possible with the new data coming from the SMC, E155 and HERMES.

The COMPASS experiment has been recommended at CERN to determine the gluon polarisation from the open charm production in the photon-gluon fusion process. The option to have polarised protons at HERA is under the study and several processes have been proposed to investigate the gluon polarisation there.

Acknowledgements

We thank the Organising Committee of the XXVII International Conference on High Energy Physics for the invitation to present this talk. This work was supported by the Polish Committee for Scientific Research (KBN) SPUB/P03/112/95 and SPUB/P03/114/96.

References

- [1] EMC, J. Ashman *et al.*, *Phys. Lett. B* **206**, 365 (1988); *Nucl. Phys. B* **328**, 1 (1989).
- [2] R.L. Jaffe, *Comments Nucl. Phys.* **19**, 239(1990).
- [3] NMC, P. Amaudruz *et al.*, *Phys. Lett. B* **295**, 159 (1992) and preprint CERN-PPE/92-124 (July 1992); Errata Oct.26(1992) and Apr.19(1993).
- [4] L.W. Whitlow *et al.*, *Phys. Lett. B* **250**, 193 (1990) and L.W. Whitlow, PhD thesis, Stanford University, 1990.
- [5] E143, K. Abe *et al.*, *Phys. Rev. Lett.* **74**, 346 (1995)
- [6] SMC, D. Adams *et al.*, *Phys. Lett. B* **329**, 399 (1994); Erratum *Phys. Lett. B* **339**, 332 (1994); F. Kunne, these proceedings.
- [7] E143, K. Abe *et al.*, *Phys. Rev. Lett.* **75**, 25 (1995).
- [8] SMC, D. Adams *et al.*, *Phys. Lett. B* **357**, 248 (1995); F.Kunne, these proceedings.

- [9] E143, K. Abe *et al.*, *Phys. Lett. B* **364**, 61 (1995).
- [10] W. Buck and F. Gross, *Phys. Rev. D* **20**, 2361 (1979); M.Z. Zuilhof and J.A. Tjon, *Phys. Rev. D* **22**, 2369 (1980); M. Lacombe *et al.*, *Phys. Rev. C* **21**, 861 (1980); R. Machleidt *et al.*, *Phys. Rep.* **149**, 1 (1987); A.Yu. Umnikov *et al.*, University of Alberta preprint Alberta-Thy-29-94, 1994.
- [11] S.A. Kulagin *et al.*, *Phys. Rev. C* **48**, R968 (1995).
- [12] H. Khan and P. Hoodbhoy, *Phys. Lett. B* **298**, 181 (1993).
- [13] EMC, P. Amaudruz *et al.*, *Nucl. Phys. B* **371**, 3 (1992); G. van Middelkoop, these proceedings.
- [14] L. Frankfurt *et al.*, hep-ph/9602301.
- [15] W. Wander, these proceedings.
- [16] E. Hughes, these proceedings.
- [17] D.M. Kawall, PhD thesis, Stanford University, 1995; S. Rock, International Workshop on DIS and Related Phenomena, Rome, 15-19 June, 1996.
- [18] E143, K. Abe *et al.*, *Phys. Rev. Lett.* **76**, 587 (1996).
- [19] H. Burkhardt and W.N. Cottingham, *Phys. Lett. B* **334**, 187 (1994).
- [20] S. Wandzura and F. Wilczek, *Phys. Lett. B* **72**, 195 (1977).
- [21] SMC, D. Adams *et al.*, *Phys. Lett. B* **336**, 125 (1994).
- [22] R. Mertig and W.L. van Neerven, *Z. Phys. C* **70**, 637 (1996); W. Vogelsang, *Phys. Rev. D* **54**, 2023 (1996).
- [23] S.D. Bass and P.V. Landshoff, *Phys. Lett. B* **336**, 537 (1994).
- [24] J. Bartels *et al.*, DESY preprint 96-25.
- [25] L. Mankiewicz *et al.*, hep-ph/9510418.
- [26] M.Meyer-Hermann *et al.* UFTP preprint 414/1996 (hep-ph/9605229); J. Ellis *et al.*, *PLB* **366**, 268 (1996).
- [27] J.D. Bjorken, *Phys. Rev.* **148**, 1467 (1966); J.D. Bjorken, *Phys. Rev. D* **1**, 1376 (1970).
- [28] J. Ellis and R.L. Jaffe, *Phys. Rev. D* **9**, 1444 (1974); *Phys. Rev. D* **10**, 1669 (1974).
- [29] S.A. Larin and J.A.M. Vermaseren, *Phys. Lett. B* **259**, 345 (1991).
- [30] A.L. Kataev and V.V. Starshenko, *em Mod.Phys.Lett. A* **10**, 235 (1995); Preprint CERN/TH 94-7198 (May 1994).
- [31] Particle Data Group, R.M. Barnett *et al.*, *Phys. Rev. D* **54**, 1 (1996).
- [32] F.E. Close and R.G. Roberts, *Phys. Lett. B* **316**, 165 (1993).
- [33] J. Ellis *et al.*, CERN preprint CERN-TH-96/188.
- [34] S.A. Larin, *Phys. Lett. B* **334**, 192 (1994).
- [35] R.D. Ball, S. Forte and G. Ridolfi, *Phys. Lett. B* **378**, 255 (1996).
- [36] T. Gehrman and W.J. Stirling, *Phys. Rev. D* **53**, 6100 (1996).
- [37] M. Glück *et al.*, *Phys. Rev. D* **53**, 4775 (1996).
- [38] SMC, B. Adeva *et al.*, *Phys. Lett. B* **369**, 93 (1996).
- [39] A.D. Martin *et al.*, *Phys. Lett. B* **306**, 145 (1993).
- [40] EMC, M. Arneodo *et al.*, *Nucl. Phys. B* **321**, 541 (1989).
- [41] X. Ji, hep-ph/9510362; hep-ph/9603249.
- [42] F. Kunne, these proceedings.
- [43] J. Feltesse and A. Schäffer, Polarisation Working Group, Workshop on *Future Physics at HERA*, Hamburg, Germany, May 1996.
- [44] M. Anselmino *et al.*, preprint DFTT 44/96 (IFT-96-16 or MPI-PhT/96-63).

^aPlenary talk presented at the XXVII International Conference on High Energy Physics, 25-31 July 1996, Warsaw, Poland.